

# Plasmonic Optical Fiber Based Continuous in-Vivo Glucose Monitoring for ICU/CCU Setup

Souvik Kundu<sup>®</sup>, Shawana Tabassum, Ritwesh A. Kumar, E. Dale Abel<sup>®</sup>, and Ratnesh Kumar<sup>®</sup>, *Fellow, IEEE* 

Abstract—This paper reports a sensor architecture for continuous monitoring of biomarkers directly in the blood, especially for ICU/CCU patients requiring critical care and rapid biomarker measurement. The sensor is based on a simple optical fiber that can be inserted through a catheter into the bloodstream, wherein gold nanoparticles are attached at its far distal end as a plasmonic material for highly sensitive opto-chemical sensing of target biomolecules (glucose in our application) via the excitation of surface plasmon polaritons. For specificity, the nanoparticles are functionalized with a specific receptor enzyme that enables the localized surface plasmon resonance (LSPR)-based targeted bio-sensing. Further, a micro dialysis probe is introduced in the proposed architecture, which facilitates continuous monitoring for an extended period without fouling the sensor surface with cells and blood debris present in whole blood, leading to prolonged enhanced sensitivity and limit of detection, relative to existing state-of-the-art continuous monitoring devices that can conduct direct measurements in blood. To establish this proof-of-concept, we tested the sensor device to monitor glucose in-vivo involving an animal model, where continuous monitoring was done directly in the circulation of living rats. The sensor's sensitivity to glucose was found to be 0.0354 a.u./mg.dl<sup>-1</sup> with a detection limit of 50.89 mg/dl.

Index Terms—Biosensor, glycemia, continuous glucose monitoring, plasmonic, SPR, LSPR.

#### I. INTRODUCTION

THERE exists technological challenges in continuous biomarker monitoring in-vivo in whole blood. These include lack of stability of the sensors and limited re-usability, reduced sensitivity due to fouling from blood debris, real-time monitoring requirement, expensive manufacturing cost, are some examples of feasibility challenges needing viable solutions [1]. In this paper, we establish a proof-of-concept

Manuscript received 1 May 2023; accepted 14 July 2023. Date of publication 7 August 2023; date of current version 3 January 2024. This work was supported in part by the National Science Foundation under Grant NSF-CSSI-2004766 and Grant NSF-PFI-2141084. (Corresponding author: Souvik Kundu.)

Souvik Kundu, Ritwesh A. Kumar, and Ratnesh Kumar are with the ECE Department, Iowa State University (ISU), Ames, IA 50011 USA (e-mail: souvik@iastate.edu; rakumar@iastate.edu; rkumar@iastate.edu).

Shawana Tabassum is with the EE Department, UT Tyler, Tyler, TX 75799 USA (e-mail: stabassum@uttyler.edu).

E. Dale Abel is with the Medicine Department, UCLA, Los Angeles, CA 90095 USA (e-mail: DOMChair\_DaleAbel@mednet.ucla.edu). Digital Object Identifier 10.1109/TNB.2023.3303345 of such a sensor architecture by targeting in-vivo continuous glucose monitoring (CGM), which is especially useful in ICUs/CCUs and where CGM becomes a critical aspect of treatment. In the case of hospitalized COVID-19 patients with pre-existing conditions of type-2 diabetes, the impact of unbalanced glucose levels is amplified, and the CGM need becomes even more given that patients with poorer blood glucose control showed an increased mortality rate relative to those with better glucose control [2].

Glycemia in critically ill ICU patients can range from hyperglycemia to hypoglycemia, where the former is not uncommon even among those patients who have not been previously diagnosed with diabetes [3]. Those cases are clinically known as stress-induced hyperglycemia (SIH), or hospital-related hyperglycemia [4], [5] and are associated with increased ICU mortality. There is also a subtle relation between sepsis [6], one of the most common causes of death in ICUs [7], and glycemic status in ICU patients. In these patients, a hyper-metabolic state exists [8], predominantly due to the intense hormonal and cytokine responses like TNF, IL-1, and IL-6, that important mediators of insulin resistance, resulting in hyperglycemia [9]. In the case of COVID-19 treatments, systemic glucocorticoids used for dampening the cytokine storm often raise blood glucose levels exponentially. This glycemic variability in the case of critically ill ICU patients is usually quantified via the standard deviation around the mean or coefficient of variation (CV), which equals standard deviation/mean [10]. Greater glycemic variability is associated with a significantly higher mortality rate: A blood glucose level standard deviation of > 20 mg/dL was associated with a 9.6-fold increase in mortality compared with a blood glucose level standard deviation of < 20 mg/dL. A study has also revealed that even a single episode of severe hypoglycemia or low glucose level is associated with an increased risk of mortality [11]. Some studies have found that glucose levels of 140-180mg/dL can be associated with the best risk-benefit ratio [12], and based on that the American Association of Clinical Endocrinologists and the American Diabetes Association have adopted these levels as targets for ICU patients [13]. Thus, continuous monitoring of glucose along with other critical ICU-relevant biomarkers is of utmost importance for the survival of critically ill ICU patients.

In this paper, we provide a sensor architecture for in-vivo continuous biomarker monitoring in blood and establish its proof-of-concept by detecting glucose. However, the approach applies to any other critical ICU/CCU biomarkers. Although there exist numerous glucose sensors (invasive, noninvasive, and minimally invasive), which can be broadly categorized as amperometric sensors, single-use with costly enzyme-based strips, or optical sensors (employing absorption spectroscopy, light scattering, or Raman spectroscopy), most of these cannot be used for continuous in-vivo monitoring in the blood due to fouling and interference caused by blood cells on the sensor surface, and the commonly used static sensor calibration is incapable of compensating for such fouling over time [14]. There exist low-fouling materials, e.g., poly(ethylene glycol) (PEG), but they also have only limited non-fouling capabilities in complex real-world media such as undiluted blood plasma and serum and its derivatives; are susceptible to oxidative damage over longer-term use; and are also difficult to directly functionalize with biomolecules for biosensing applications [15], [16]. Also, the wearable sensors integrated with bio-needles for measuring glucose continuously in sweat or other subcutaneous body fluids can lack a proper correlation with the immediate blood glucose concentration.

Fiber-optic sensors enjoy unique advantage for in-vivo monitoring in while blood, that those can be inserted through patient's catheter into the blood stream in ICU/CCU setting, and while different types of gold nanoparticles coated optical fiber-based glucose sensors are reported in the literature [17], [18], they are incapable of providing continuous in-vivo monitoring of glucose for a prolonged period due to fouling caused by the proteins, cells, and other interfering molecules present in the blood.

In contrast to these previous works that mainly focus on sensor design, our work advances the existing state-of-art in in-vivo glucose sensor design by integrating the fiber-tip sensor with a microdialysis probe for continuous glucose monitoring in whole blood for a prolonged period: In our sensing architecture, we have proposed the integration of a microdialysis ( $\mu$ D) probe with 20kDa membrane molecular weight cutoff (MWCO) to prevent the sensor from coming in direct contact with the larger blood molecules and thereby reduce its fouling. Integration of the microdialysis probe not only protects the sensor from fouling but also enables easy access to whole blood for continuous monitoring in an existing ICU/CCU setup: The functionalized opto-chemical fiber sensor can be inserted inside a microdialysis probe, and the entire assembly can be inserted through a patient's catheter that is already furnished in an ICU/CCU setup, thereby avoiding any extra logistic or overheads. We have established this proof-ofconcept by doing live experiments in a live rat as narrated in the subsequent sections.

The main novelties of our work are:

- nano-sensing footprint of the fiber optic cable that makes
  it amenable for insertion into the bloodstream through
  a catheter for in-vivo monitoring in critical care setting
  without any extra logistics, and
- integration of the fiber-tip sensor with a microdialysis probe that allows continuous in-vivo monitoring in whole blood for a prolonged period. We have demonstrated a

proof of concept by testing the integrated sensing system in a live rat, mimicking the ICU/CCU setup.

Summarily, the paper provides these contributions:

- Detailed fabrication process for the opto-chemical fiber optic sensor.
- Measurements exploiting localized surface plasmon resonance of the sensor and evaluation of sensitivity, LOD of the sensor.
- An integrated micro dialysis probe based in-vivo measurement for continuous glucose monitoring in living rats.
- Performance comparison of the proposed sensor against the continuous glucose monitoring sensors reported in the literature.

#### II. PLASMONIC SENSOR WORKING PRINCIPLE

This section describes the working mechanism of the gold nanoparticle-coated optical fiber sensor probe. Given that an in-vivo detection requires a reflected (as opposed to transmitted) signal for measurement, the sensor is made on the far distal end of a fused bifurcated fiber (see Fig 1) that can be inserted through a catheter into the bloodstream. Gold nanoparticles (AuNP) are deposited as shown in Fig 1 (in the form of red dots) to provide for localized surface plasmon resonance (LSPR). Light guided through the optical fiber interacts with the AuNPs at the far distal end of the fiber and excites the surface plasmons (valence bonded electrons). At the LSPR wavelength, the incident light has maximum absorption (equivalently, minimum reflected intensity). The LSPR wavelength depends on the AuNP characteristics (material, size, shape, refractive index (RI)), and RI of the local surrounding medium—This is formalized below in Section II-A. Accordingly, a change in local surrounding medium RI results in a shift in resonance wavelength and also a change in the absorption level (and so also the reflected intensity level) at the original resonance wavelength. We propose to measure intensity variations as opposed to resonance wavelength shifts because the sensors basd on localized surface plasmon have been reported to have reduced sensitivity in wavelength modulation configuration and hence the intensity modulation configuration is preferred [19]. For the specific detection of glucose molecules, the AuNP coated fiber is functionalized with glucose oxidase (GOx) enzyme (see the yellow Y's in Fig 1). During the glucose detection on the AuNP surface, the glucose trapped within the immobilized GOx enzyme gets oxidized by enzymatic reaction, producing gluconic acid and hydrogen peroxide as the products (see the dark and light blue dots in Fig 1) and changing the local surrounding medium RI. The effect of this on the refractive index change is then detected as an intensity change at the LSPR wavelength [17].

#### A. Theoretical Formulation of the Sensing Mechanism

The proposed fiber optic-based LSPR sensor system comprises three layers:

• Fiber core made up of silica (SiO<sub>2</sub>) of refractive index, say  $\eta_0$ .

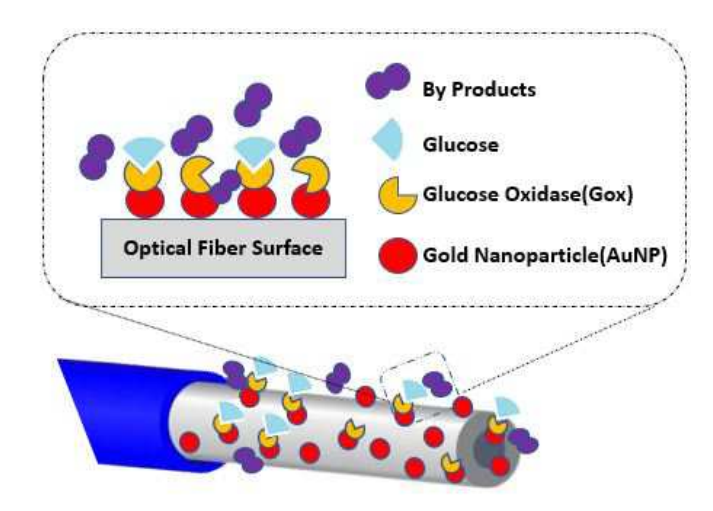


Fig. 1. Fiber optic LSPR based glucose sensing principle.

• Metallic (Au) nanoparticle layer, whose real part of dielectric constant  $\epsilon_r$  is given by (1) [20]:

$$\epsilon_r = 1 - \frac{\lambda^2}{\lambda_p^2},\tag{1}$$

where  $\lambda_p$  is the plasma wavelength of the electrons in the metal nanoparticle layer, and  $\lambda$  is the wavelength of the incident light.

• Target sensing layer, whose dielectric constant and refractive index are denoted  $\epsilon_s$  and  $\eta_s$ , respectively. (In this paper, the target sensing layer consists of GOx at its base that traps and oxidizes glucose.)

Fundamentally, surface plasmon resonance (SPR) is the oscillation resonance of the valence electrons in metal layers induced by incident radiation of an appropriate frequency. When this phenomenon is observed in nanoscale particles/layers, it is called localized surface plasmon resonance (LSPR). The mathematical formulation of the resonance condition and an expression for LSPR wavelength are presented next.

## B. Resonance Condition

The wave incident at the core and metallic nanoparticle layer interface can undergo extinction (E), transmission (T), and reflection (R). Since, in our optical fiber design, the light gets totally internally reflected at its far end, there is no transmission component, i.e., a part of the wave gets extinct due to the absorption and scattering by the nanoparticles, and the rest gets reflected for measurements. Thereby the reflected spectrum shows a dip at a wavelength where the extinction is maximum due to LSPR. For very small particles of diameters (d) less than wavelength of incident light, the scattered fields produced by a plane wave incident on a homogeneous conducting sphere (AuNPs in our case) results in the following extinction, scattering, and absorption components, given by (3), (2), and (4) respectively [21], [22]:

$$E_{ext} = \frac{2\pi}{|k|^2} \sum_{L=1}^{+\infty} (2L+1)[Re(a_L+b_L)],$$
 (2)

$$E_{sca} = \frac{2\pi}{|k|^2} \sum_{L=1}^{+\infty} (2L+1)[|a_L|^2 + |b_L|^2], \tag{3}$$

$$E_{abs} = E_{ext} - E_{sca}, (4)$$

where k is the incident wave-vector, L values are integers representing the dipole, quadrupole, and higher multipoles of the scattering, and finally,  $a_L$  and  $b_L$  are composed of the Riccati-Bessel functions [22]. In case of spherical AuNPs, L=1, and the  $a_L$  and  $b_L$  values for L=1, as approximated from power series, are given by (5):

$$a_{1} = \frac{(kd)^{3}}{12} \left( \frac{-i\epsilon_{r}^{2} - i\epsilon_{r}\epsilon_{s} + 3\epsilon_{i}\epsilon_{s} - i\epsilon_{i}^{2} + i2\epsilon_{s}^{2}}{(\epsilon_{r} + 2\epsilon_{s})^{2} + (\epsilon_{i})^{2}} \right),$$

$$b_{1} \approx 0,$$
(5)

where  $\epsilon = \epsilon_r + i\epsilon_i$ , with  $\epsilon_r$  being the real part and  $\epsilon_i$  being the imaginary part of the metallic nanoparticle dielectric function, and  $\epsilon_s$  is the dielectric constant of the surrounding medium. Substituting (5) into (2) and retaining only the L=1 term yields (6):

$$E_{ext} = \frac{3\pi d^3 \epsilon_s^{\frac{3}{2}}}{2} \frac{\epsilon_i}{(\epsilon_r + 2\epsilon_s)^2 + \epsilon_i^2}.$$
 (6)

Similarly,  $E_{sca}$  can be evaluated by substituting (5) into (3). The extinction in (6) is maximized when the denominator is minimized, and that condition is met when  $\epsilon_r = -2\epsilon_s$  assuming  $\epsilon_i$  is small or only weakly dependent on the wavelength of the incident light. This explains the dependence of the LSPR absorption peak on the surrounding environment. Substituting  $\epsilon_r = -2\epsilon_s$  (resonance condition) and  $\epsilon_s = \eta_s^2$  in (1), we obtain the expression for the LSPR wavelength (7):

$$\lambda_{\rm LSPR} = \lambda_p \sqrt{2\eta_s^2 + 1}.\tag{7}$$

#### III. SENSOR FABRICATION AND FUNCTIONALIZATION

This section narrates the detailed steps to fabricate the fiber optic-based LSPR sensor probe. There are three basic steps to the fabrication as follows:

- 1) Preparation of  $\sim$ 10 nm radius spherical gold nanoparticles.
- 2) Immobilization of the nanoparticles on the fiber surface.
- 3) Functionalization of glucose oxidase on the immobilized nanoparticles.

These steps are also depicted in Fig. 2. The integration of the sensor with a  $\mu D$  probe is discussed in Section IV-B.

# A. Synthesis of ~10 nm Radius Gold Nanoparticles

1 mM and 38.8 mM aqueous solutions of HAuCl<sub>4</sub> and trisodium citrate were prepared, respectively. 10 mg of HAuCl<sub>4</sub>.3H<sub>2</sub>O was mixed in 50 ml of DI water, and 500 mg of Sodium Citrate was mixed in 50 ml of DI Water. 20 ml of aqueous solutions of HAuCl<sub>4</sub> was poured into a beaker at  $200^{\circ}$  C and constantly stirred at 500 rpm. As soon as the boiling started, trisodium citrate solution was added such that the volume ratio of the two solutions was HAuCl<sub>4</sub>: citrate = 10: 1. (The size of the gold nanoparticles can be

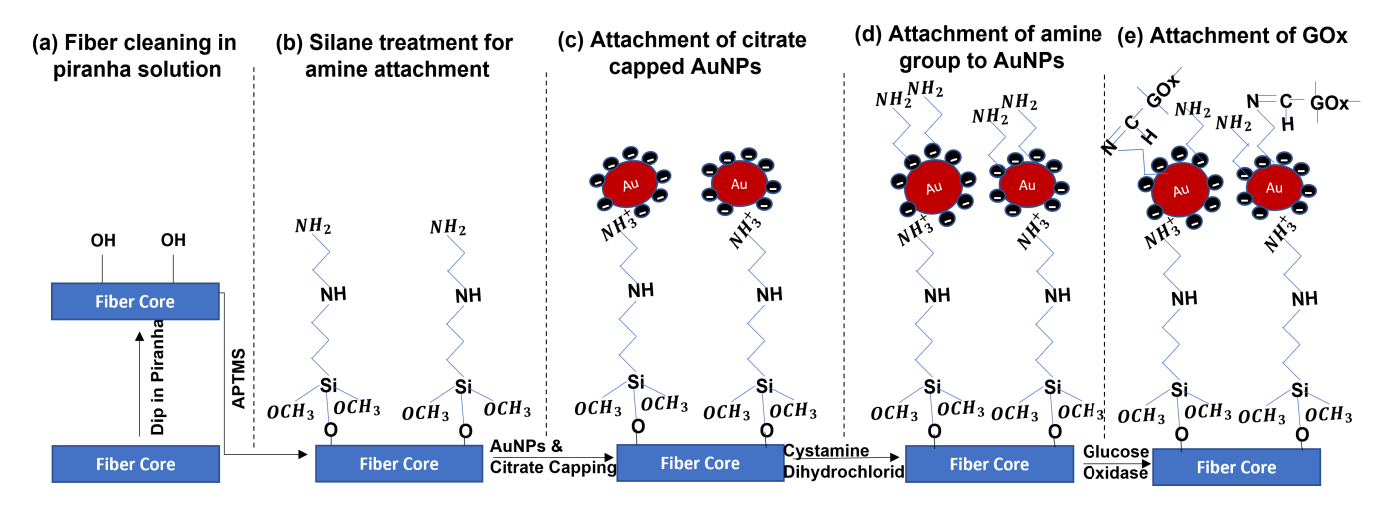


Fig. 2. Sensor fabrication steps. (a)-(c) Illustrate the process of AuNP attachment on the sensor surface; (d)-(e) Illustrate the GOx functionalization on AuNPs by amine linker.

modulated by changing the molar ratio of HAuCl<sub>4</sub> to trisodium citrate. Typically, AuNPs between 10 nm and 150 nm radii can be synthesized by adjusting the molar ratio, and the chosen ratio was to attain the desired 10 nm size.) A violet-colored liquid appeared quickly, transforming to a bright red after 30 minutes of boiling and stirring when HAuCl<sub>4</sub> was reduced by trisodium citrate. After that we stopped the boiling and stirred the solution until it was brought to room temperature (approximately 30 minutes) and gold nanoparticles thus formed was stored at room temperature until use. A detailed study has been presented in [23], which is what we adopted.

# B. Fabrication of the Nanoparticle-Coated Sensor on the Far Distal End of the Fiber

First, the external polymer jacket of the fiber at its tip was removed using a fiber optic stripper. Next, approximately 3-4 cm of the cladding of a multimode fiber was removed from its far distal end using an acetone-soaked Kimwipe by a multi-step stripping procedure dipping the fiber into acetone for 20 min. The cladding part starts to dissolve in acetone, making the stripping of the cladding easier. The distal end of a multi-mode fiber (with a core diameter of 200  $\mu$ m) was cut with a fiber cutter to create a flat tip. The unclad sensing area was next cleaned and hydrolyzed with Piranha solution (volume ratio of  $H_2SO_4$ :  $H_2O_2 = 7$ : 3) for 30 min at 85° C, which provided -OH groups on the fiber surface as shown in Fig. 2(a). Next, the sensing region of the optical fiber was rinsed with DI water, blow-dried with N2, and annealed in a vacuum oven for 30 min at 110° C then immersed in a 10% solution of 3-aminopropyl trimethoxysilane (APTMS) in methanol for 1 hr. at 40° C, which provided a monolayer of -NH<sub>2</sub> groups on the fiber surface as illustrated in Fig. 2(b). The fiber was next rinsed sequentially with ethanol and DI water to remove unbound APTMS, blow-dried with N2, and again annealed in a vacuum oven for 30 min at 110° C. The sensing region was then incubated in a gold nanoparticle solution overnight. Afterwards, the fiber was washed with DI water to get rid of any unbound nanoparticles and dipped back

in the nanoparticle solution for 12 hours to ensure effective attachment of the nanoparticles on the fiber surface, as seen in Fig. 2(c).

Note while ~10 nm sized AuNPs predominately occur during the above-described synthesis process of Section III-A, there may still exist AuNPs of smaller radii, which hardly contribute to LSPR. Hence, even after the AuNP attachment on the fiber surface, there is a possibility of improved LSPR signal by in-situ growth of the smaller AuNPs using, for example, a process described in [24] and [25]. In that case, the fiber needs to be immersed in 1 mM sodium citrate dehydrate aqueous solution for 5 min, where the citrate ions help accumulate the AuNPs, thereby facilitating the growth of the smaller radius AuNPs. Note this is an optional step that can be employed in case the LSPR signal of the designed probe turns out to be low.

#### C. Sensor Functionalization

To attach the glucose oxidase enzyme to the sensor surface, first a 20  $\mu$ M solution of glucose oxidase in 0.1 M sodium phosphate buffer (6.8 pH) was prepared and kept at 4° C. 30 mg sodium metaperiodate was added and mixed continuously for 1 hour in an ice bath made in a Styrofoam cup (rather than with a conventional immersion cooler system) to maintain the reaction temperature at  $0^{\circ}$  C. 6.97  $\mu$ l of ethylene glycol was added to stop the reaction and it was followed by vigorous 30 minutes stirring. To attach the glucose oxidase enzyme to the sensor surface, the fiber optic sensor was first dipped in a 1 mM aqueous solution of cystamine dihydrochloride for 1 hr. This created a monolayer of amine groups on the nanoparticle-coated fiber as depicted in Fig. 2(d). The probe was then immersed in a glucose oxidase solution for 12 hrs, allowing the modified glucose oxidase to bind to the -NH<sub>2</sub> groups. After rinsing the fiber probes with DI water to discard any unbound species, they were incubated in the glucose oxidase solution for 12 hrs. This ensured effective binding of the glucose oxidase to the nanoparticles on the fiber probe as depicted by Fig. 2(e).

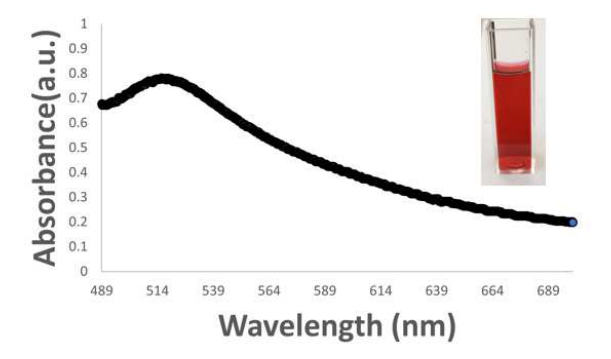


Fig. 3. Absorbance spectrum of AuNP of average diameter between 10 and 20 nm and maximum absorbance at 514 nm. Inset shows the corresponding gold nanoparticles.

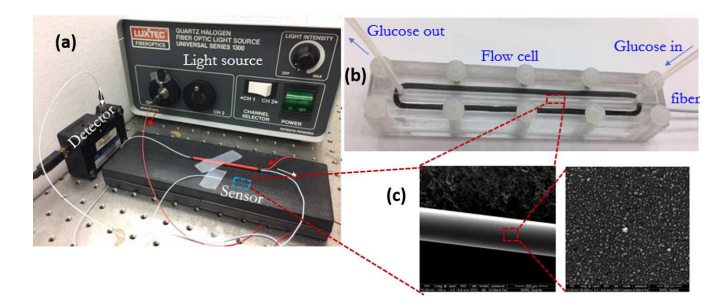


Fig. 4. Experimental setup at ESSeNCE Lab, ISU. (a) Illustrates the light source and detector along with the fused fiber with the fabricated sensor at its far distal end. (b) Glucose measurement setup in flow cell. (c) Illustrates the SEM image of the gold nanoparticles after attaching them on the optical fiber surface.

# IV. LSPR CHARACTERIZATION AND EXPERIMENTAL VALIDATION

After fabricating a gold nanoparticle (AuNP)-coated optical fiber sensor probe for in-vivo glucose detection in blood, the AuNPs were characterized using a UV-VIS spectrophotometer by observing the absorption spectrum as shown in Fig. 3. The peak absorption was observed at 514 nm, which confirms that the nanoparticles have an average diameter between 10 nm to 20 nm, in accordance with the fabrication process and the underlying theory [26]. The scanning electron microscope image in the inset of Fig. 4(c) further confirms the successful attachment of AuNPs to the fiber surface (using (3)-aminopropyl)trimethoxysilane linkers).

#### A. Glucose Monitoring Validation in Buffer Solution

Fig. 4(a) depicts the optical sensor's experimental validation setup, consisting of a broadband white light source, an optical detector (range 400 nm to 750 nm), and a  $2 \times 1$  fused optical fiber. The light source illuminates the sensing element of approximately 4 cm length toward the far distal end of the optical fiber. Light reflected off the element is detected by the detector, and its spectrum is recorded. The response of the sensor to glucose was independently validated before its in-vivo use by employing a flow cell around the sensing element (shown in Fig. 4(b)) through which distilled water-based solutions of various glucose concentrations (within 0-250 mg/dL range) were passed, and the corresponding reflection spectra

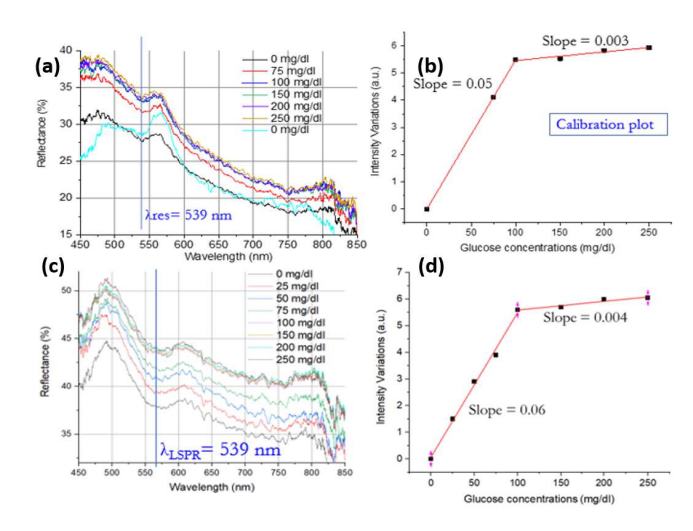


Fig. 5. (a) Reflection spectrum in static glucose solution. (b) Calibration curve in static glucose solution. (c) Reflection spectrum in flow cell (d) Calibration curve in a flow cell.

were recorded as shown in Fig. 5 (the plots of the figure are discussed in Section V-A.)

#### B. Continuous Glucose Monitoring in Live Rats

Figure 6 shows the experimental setup for CGM in a live rat, along with the schematics of a bypass circuit to flow the blood through the sensor. To prevent the optical sensor from fouling secondary to sample deposition and coagulation, the sensor was inserted into a  $\mu D$  probe (MWCO 20kDa), chosen in accordance with and higher than the molecular weight of glucose. With the use of a  $\mu D$  probe with MWCO 20kDa, all bigger molecules having sizes higher than 20kDa get filtered, thereby preventing the fouling of the sensor probe and also reducing the non-specific bindings to a great extent, and eventually helping in enhancing the longevity, sensitivity, and specificity of the sensor.

There are seven main "points" of the by-pass circuit as labeled alphabetically in the schematic diagram of Figure 6. Point A depicts blood flow from the rat's right jugular vein into the surgically set bypass circuit. Point B is periodically opened and closed to sample blood from the bypass circuit to obtain the reference values of the blood glucose concentration from a commercial glucometer. At Point C, a 3-way T-junction is placed to reroute the blood back into the rat, and the  $\mu D$  probe is placed at this junction, as shown in the figure to allow only the blood components less than 20kDa to pass through the  $\mu D$ membrane while blocking the larger ones. Point D is an inlet made available for occasional washing of the external surface of the  $\mu D$  to remove any blood debris clinging onto the probe surface. At point E, the blood flows back into the jugular vein of the rat, thereby completing the bypass loop. The  $\mu D$  probe has one inlet (Point F) and one outlet (Point G). The inlet Point F is fed with heparin as a perfusion fluid, which prevents blood from clotting at the interface of the  $\mu D$  membrane, through which the glucose molecules percolate into the  $\mu D$  probe. The heparin solution, which has zero initial glucose concentration, creates a concentration gradient at the blood-micro dialysis

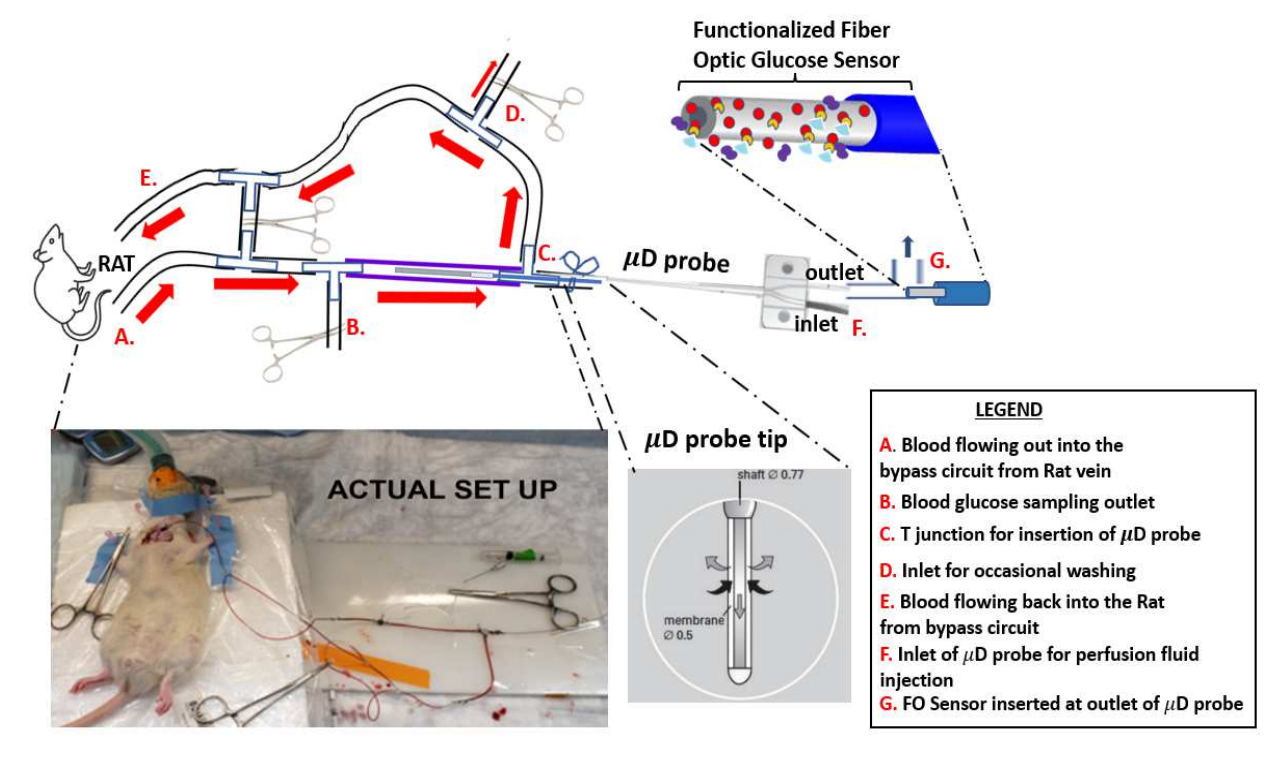


Fig. 6. Experimental Setup for continuous glucose monitoring (CGM) on a live rat.

membrane interface, which helps in the movement of glucose molecules from higher concentration (in the blood) to lower concentration (in heparin) across the membrane. Thus, the exiting heparin distillate contains glucose molecules which we detect at the outlet of the  $\mu D$  probe using our proposed optical fiber-based LSPR sensor.

During the measurement, the blood glucose level (BGL) was adjusted in the rat by managing the insulin and the glucose infusion rates via the right jugular catheter. For a normal rat with insulin flow at 2.5 mU/min/kg, we observed that a typical glucose infusion rate of about 55-60 mg/kg/min is needed to maintain the BGL steady at its initial value.

#### C. Instruments and Reagent Sources

For the measurements, a quartz halogen lamp which is a white light source of power 150-watt (Luxtec Fiber Optics, Plainsboro, NJ) was connected to  $1 \times 2$  Multimode Fiber Optic Coupler, High OH, Ø200 µm Core, 0.39 NA, 50:50 Split, FC/PC. The reflected light from the fiber optic sensor tip was measured by a UV/VIS spectrometer (USB-4000, Ocean Optics) that is connected to the other end of the optical coupler. Syringe pumps were used to inject the glucose solution into the flow cell for experiments in buffer solution and for injecting the perfusion fluid through the inlets of the  $\mu D$  probe. HAuCl<sub>4</sub>, tri-sodium citrate, 3-aminopropyl trimethoxysilane (APTMS), sodium metaperiodate, GOx and cystamine dihydrochloride were procured from Sigma-Aldrich. Sulfuric acid, hydrogen peroxide, methanol and DI water were obtained from Chemstore, ISU. Mouse blood was procured from Biochemmed, Winchester, VA.

#### V. RESULTS AND DISCUSSIONS

To establish a proof-of-concept, we studied the behavior of the proposed sensor architecture for in-vitro (in flowing buffer solution) as well as in-vivo (in live rat) glucose detection. This section discusses the corresponding measurement results.

# A. Sensor Characterization in Buffer Solution

The measurement results were obtained at the ESSeNCE Lab., ISU, where we tested the performance of the sensor in three different settings: (i) static glucose solution, (ii) in a flow cell with PBS buffered glucose solution, (iii) in mouse blood. A post-meal blood glucose level in a non-diabetic, should be < 180 mg/dl, and a pre-meal glucose level can range from 90 to 130 mg/dl. Hence, we tested for a concentration range of 0-250 mg/dl. The results in Figure 5(a)-(b) correspond to the measurements of dipping the sensing tip into still solutions of glucose. We observed sensitivity of 0.05 a.u./mg.dl<sup>-1</sup> at glucose concentrations of 0 to 100 mg/dl, and 0.003 a.u./mg.dl<sup>-1</sup> at glucose concentrations of 100 to 250 mg/dl.

Fig. 4(b) illustrates a flow cell setup that we used to take readings of glucose in a flowing buffer solution. Fig. 5(c)-(d) depicts the performance of the fiber optic sensor in the flow cell, which shows nearly the same sensitivity both at lower and higher glucose concentrations. (Sensitivity of 0.06 a.u./mg.dl<sup>-1</sup> was obtained at lower concentration of glucose between 0 to 100 mg/dl, and of 0.004 a.u./mg.dl<sup>-1</sup> at higher concentration of glucose between 100 to 250 mg/dl.)

Since, in a real ICU/CCU scenario, glucose concentrations have to be measured in whole blood, we studied our sensor's

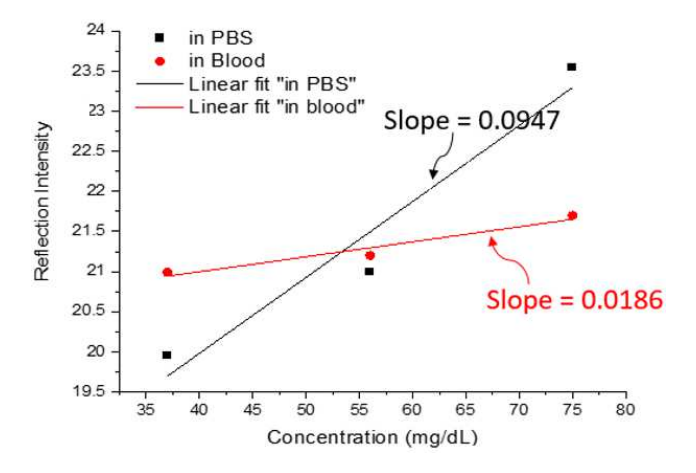


Fig. 7. Sensor performance comparison in PBS buffer vs. mouse blood.

sensitivity and LOD in mouse blood to imitate the behavior of the sensor's response in the presence of blood debris. Fig. 7 depicts that response, and although there is an expected reduction in sensitivity and LOD in blood solution compared to the case of PBS buffer solution, the sensor remains capable of detecting a very low glucose concentration in blood samples. The LOD of the sensor in the blood sample is 15.3 mg/dl, which, although higher than the 2.59 mg/dl level of LOD in the PBS buffer solution, is still well below the normal lower limit of glucose concentration in a human being.

## B. Sensor Characterization in Blood From Live Rats

The results obtained in the live rat model are reported in this section. The experimental environment is set by establishing a stable insulin infusion rate via a right jugular venous catheter, aiming to reach a steady state of plasma insulin. At the same time, to maintain stable blood glycemia at the desired level, we infused 50% glucose via the same catheter placed in the rat's right jugular vein at various variable flow rates. For a normal rat with insulin flow at 2.5 mU/min/kg, we typically needed glucose infusion rates of about 55-60 mg/kg/min. We performed this dyad of insulin and glucose infusion to regulate the blood glucose level of the rat to imitate the blood glucose range of 80 to 250 mg/dl as in the case of a human. This helped us to test our sensor in a similar setting which may prevail in an ICU. During the assay, we also manually collected blood for measuring glucose using a glucometer to independently obtain data for the sensor calibration. Fig. 8 depicts the entire response spectrum of the fiber optic sensor at different glucose concentrations.

For a stability and repeatability study, the measured spectra at different glucose concentrations (between 100 to 315 mg/dl) are illustrated in Fig. 9 for three different sensors. Based on the shift in intensity values at different glucose concentrations, calibration curves, chosen to be monotonically increasing functions (to guarantee 1-1 mapping essential for calibration), are fitted for all three sensors. The fitted curve for sensor1 is given by: y = 37.73 + 0.03769x with  $R^2 = 0.77$ ; for sensor2 it is given by y = 40.57 + 0.03357x with  $R^2 = 0.81$ ; and for sensor3 is given by: y = 39.35 + 0.03497x

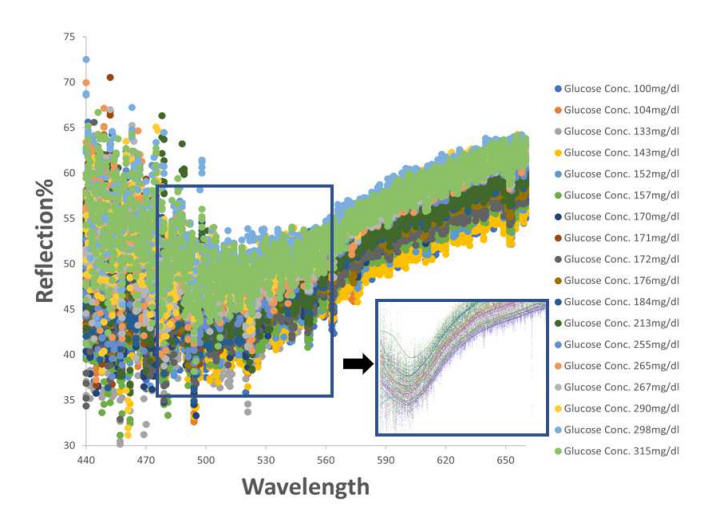


Fig. 8. Raw reflection spectra for different glucose concentrations.

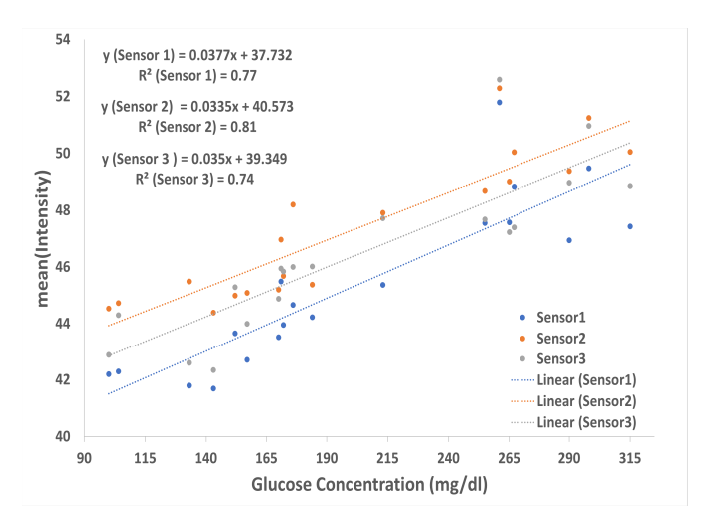


Fig. 9. Stability and repeatability analysis.

with  $R^2=0.74$ . The sensitivities of all three sensors are comparable as it varies between 0.033 to 0.037. A combined calibration curve is derived from the three individual sensor curves as shown in Fig. 10 and is given by y=39.298+0.0354x with  $R^2=0.7989$ . This corresponds to an overall sensitivity of 0.0354 a.u./mg.dl<sup>-1</sup>, using which, the limit-of-detection is determined to be, LOD =  $\frac{3\times SD}{\text{sensitivity}} = \frac{3\times0.600513}{0.0354} = 50.89$  mg/dl. The coefficient of variation (C.V.) at different glucose concentrations is given in Table I, and found to be less than 2.5% on average.

Fig. 12 depicts the sensor response over 2 hrs when the glucose concentration was varied dynamically (red dots and the fitted red curve) and the resulting reflection% was captured (blue dots and the fitted blue curve). From the two curves, it is clear that the sensor responded linearly as expected from its linear calibration curve of Figure 10. The sensor response is nearly real-time with a small delay of only about 2 min on average, as opposed to a lab test for certain biomarkers that can be time-consuming, making it non-real-time. The sensor delay is due to the time taken for the glucose to profuse through the microdialysis membrane and for its oxidation to occur. Through rigorous experiments, we observed that the sensor

TABLE I
COEFFICIENT OF VARIATION (C.V.) AT DIFFERENT GLUCOSE CONCENTRATIONS

Glucose Conc. (mg/dl)	100	104	133	143	152	157	170	171	172	176	184	213	255	261	265	267	290	298	315
Coeff. of Variance (CV)	2.78	2.95	4.48	3.28	1.94	2.71	1.99	1.63	2.31	3.86	2.01	3.01	1.29	0.77	1.97	2.71	2.68	1.88	2.68

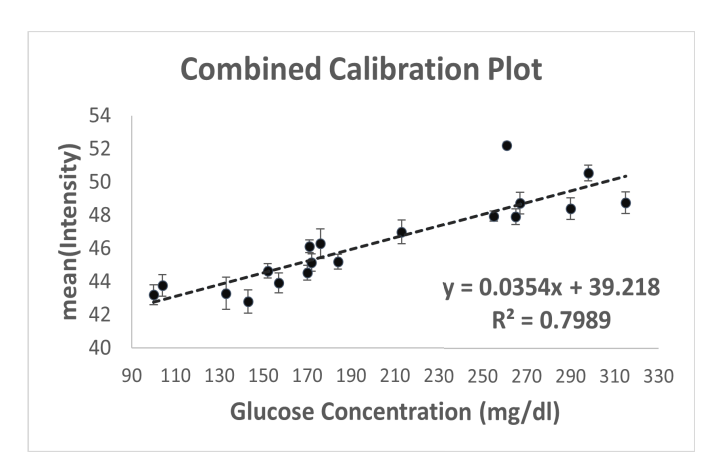


Fig. 10. Combined calibration curve in whole rat blood.

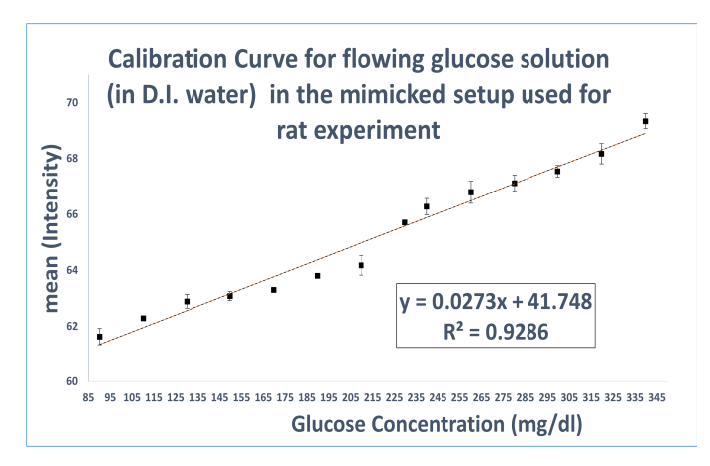


Fig. 11. Sensor calibration curve when glucose spiked DI water was flown over the sensor in an ICU/CCU mimic setup.

response delay can be reduced by pre-soaking the sensor in a buffered glucose solution prior to using it. Similarly, the delay incurred in profusion can be reduced by using a higher-quality microdialysis probe. The R-squared value of the sensor in whole blood of 0.79 as depicted in Figure 10 lies within the 0.75-0.9 range, indicating that the sensor data is of good quality and is reliable [27]. Also, we only used simple-minded static calibration for this study, whereas with a more sophisticated dynamic calibration, the R-squared value is expected to be higher, and the development of dynamic calibration is part of our ongoing study [28]. Indeed to validate that there is room for better fit through a more sophisticated calibration, we evaluated the sensor's nascent performance by fabricating and testing identical sensors, where the ICU setup circuit was mimicked by using a set of syringe pumps, and glucose spiked D.I. water of varying concentrations was flown over the sensor for measurements. The resulting calibration curve of Fig.11 depicts the R-squared value of 0.92, with

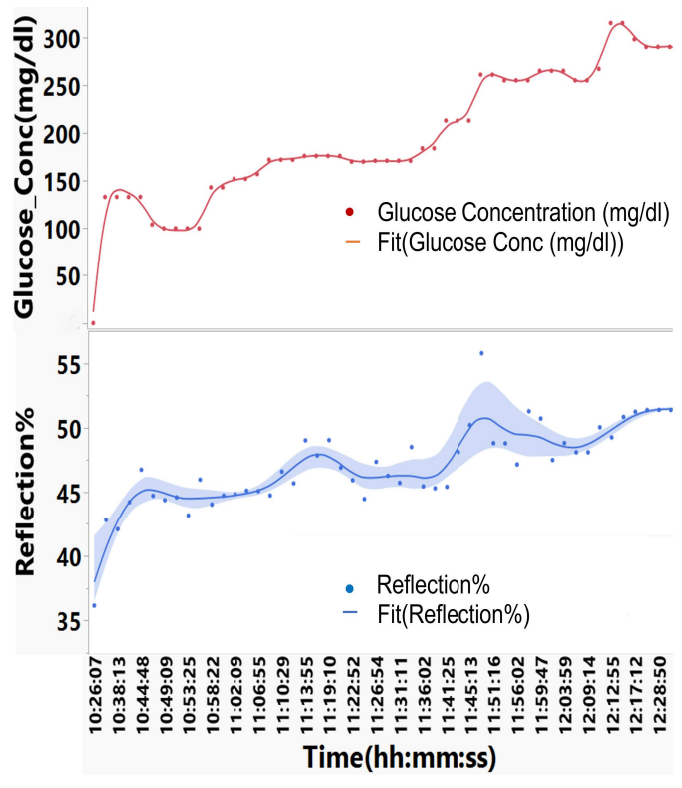


Fig. 12. Sensor dynamics for in-vivo continuous glucose monitoring: glucose profile (top) vs. sensor response (bottom).

low error bars. Also, another direction of sensor quality enhancement is by improving the quality of the microdialysis to filter out molecules with even lower molecular weights than the current 20kDa, which again is a topic of further study, inspired by the success of the proof-of-concept of the current design.

#### VI. PERFORMANCE COMPARISON

We compared the overall performance, merits, and complexity of the proposed sensor architecture with the existing state-of-the-art fiber optic glucose sensors, as shown in Table-II. The proposed sensor was tested for glucose concentrations ranging between 90 and 315 mg/dl in whole blood. The sensor's calculated limit-of-detection (LOD) is 50.89 mg/dl, meaning it can cover the glucose concentration range found in human blood (i.e., between 50 to 315 mg/dl), which bolsters the utility of the sensor for use in humans. There exist other sensors with larger range or higher sensitivity, but except for one, none are capable of in-vivo monitoring; plus, our sensor has an advantage over others due to the integration of  $\mu$ D probe, providing a prolonged period of in-vivo continuous measurement ( $\sim$ 2 hrs.) without requiring any extra processing steps such as separation of plasma or

Sensor type	Measurement range (mg/dl)	Sensitivity (a.u./mg.dl <sup>-1</sup> )	Measurement Type	Analyte	References
MM Microfiber with APTES	0-300	0.0174	In vitro	SA buffer, horse, and calf serum	[29]
Graphene Oxide modified TFG	0-144	0.24	In vitro	DI Water	[30]
Nafion and Enzyme coated electrode	56.210-108.069	0.022	In vivo	Whole Blood	[31]
Enzyme based needle electrode	70-420	3.10	In vitro	Interstitial Fluids, Fish blood	[32]
Fiber Optic SPR with MEA	0-500	0.854	In vitro	SA buffer	[33]
Fiber Optic SPR and enzyme	0-400	3.10	In vitro	DI Water, Urine	[34]
Back-scattered MIR spectroscopy	80-160	not reported	In vivo	Skin interstitial fluid	[35]
Transmission MIR spectroscopy	75-600	not reported	In vivo	Trans-cutaneous	[36]
LSPR with APTMS and Glucose Oxidase	90-315	0.0354	In vitro, In vivo	PBS Buffer and Whole Blood	This work

TABLE II
PERFORMANCE COMPARISON

serum, thereby reducing it's complexity. Most other continuous monitoring sensors reported in the literature do not measure glucose directly in blood and thus require extrapolation to correlate the blood glucose with that in the tissue fluid, making those not fully accurate or real-time. Further, in our design, the fabrication steps are relatively simpler, mostly involving standard chemical processing without the need for complex deposition techniques or equipment.

#### VII. CONCLUSION

In summary, this paper presents an LSPR-based fiber optic opto-chemical sensor for continuous glucose monitoring in whole blood for 2 hrs. of unimpeded operation. The work reported a sensor architecture integrating a micro-dialysis probe for preventing the fouling of the sensor surface in the operational period, and minimizing non-specific signal output, thereby improving accuracy and offering better SNR. The designed sensor architecture was validated in buffer as well as in an animal model, producing a proof-of-concept for future development of fiber optic multiplexed sensors, targeting multiple biomarkers in whole blood for continuous monitoring in ICU/CCU settings. The good repeatability of the sensor demonstrates the robustness of the proposed design for prolonged continuous biomolecular detection directly in whole blood. The proposed methodology involves the detection of variations in intensity in the visible light range, allowing integration of an inexpensive source and detector to make a portable, cost-effective point-of-care detector for biomarker continuous tracking in real-time, making the design amenable to scaling for mass production.

While the integration of  $\mu D$  probe prolongs the life of the sensor by blocking the deposition of larger blood-borne molecules on the sensor surface, smaller blood-borne molecules can still slowly deposit on the sensor probe, causing its response to drift slowly over time. To further prolong the

sensor life for continuous monitoring applications, a sensor re-calibration will be required, that may interfere with the ability to do continuous monitoring [37], [38]. This situation can be addressed by developing a generalized time-dependent calibration model capable of also correcting for any time drift in sensor response. We refer to such an approach as "dynamic calibration", where not just the current sensor response but also its historic readings are used for adjusting the calibration. The details of its mathematical formulation are reported in our paper [28], where we have proposed a Bayesian framework for dynamic calibration of sensors using the history of sensor measurements and the observed ground truth data.

#### **ACKNOWLEDGMENT**

The authors would like to thank the Electronics Technology Group, Electrical and Computer Engineering, Iowa State University (ISU) for assistance with logistics support toward design of experiments; the Materials Analysis and Research Laboratory, ISU, for imaging support; and Wojciech Jacek Grzesik and Kyle Bradberry at the Metabolic Phenotyping Core Facility, University of Iowa, for the animal model experimental setup and execution.

## REFERENCES

- [1] H. Zafar, A. Channa, V. Jeoti, and G. M. Stojanović, "Comprehensive review on wearable sweat-glucose sensors for continuous glucose monitoring," *Sensors*, vol. 22, no. 2, p. 638, Jan. 2022.
- [2] L. Zhu et al., "Association of blood glucose control and outcomes in patients with COVID-19 and pre-existing type 2 diabetes," *Cell Metabolism*, vol. 31, no. 6, pp. 1068–1077, 2020.
- [3] C. S. Levetan, M. Passaro, K. Jablonski, M. Kass, and R. E. Ratner, "Unrecognized diabetes among hospitalized patients," *Diabetes Care*, vol. 21, no. 2, pp. 246–249, Feb. 1998.
- [4] P. J. Palumbo, "Blood glucose control during surgery," J. Amer. Soc. Anesthesiol., vol. 55, no. 2, pp. 94–95, Aug. 1981.
- [5] J. J. Pomposelli et al., "Early postoperative glucose control predicts nosocomial infection rate in diabetic patients," J. Parenteral Enteral Nutrition, vol. 22, no. 2, pp. 77–81, Mar. 1998.

- [6] S. Kundu, S. Tabassum, and R. Kumar, "A perspective on sepsis pathogenesis, biomarkers and diagnosis: A concise survey," *Med. Devices Sensors*, vol. 3, no. 4, p. e10089, 2020.
- [7] S. Kundu, S. Tabassum, and R. Kumar, "Plasmonic point-of-care device for sepsis biomarker detection," *IEEE Sensors J.*, vol. 21, no. 17, pp. 18837–18846, Sep. 2021.
- [8] K. C. McCowen, A. Malhotra, and B. R. Bistrian, "Stress-induced hyperglycemia," Crit. Care Clinics, vol. 17, no. 1, pp. 107–124, Jan. 2001.
- [9] B. A. Mizock, "Alterations in fuel metabolism in critical illness: Hyperglycaemia," *Best Pract. Res. Clin. Endocrinol. Metabolism*, vol. 15, no. 4, pp. 533–551, Dec. 2001.
- [10] J. S. Krinsley, "Glycemic variability: A strong independent predictor of mortality in critically ill patients," *Crit. Care Med.*, vol. 36, no. 11, pp. 3008–3013, Nov. 2008.
- [11] J. S. Krinsley and A. Grover, "Severe hypoglycemia in critically ill patients: Risk factors and outcomes," *Crit. Care Med.*, vol. 35, no. 10, pp. 2262–2267, 2007.
- [12] J.-C. Preiser and P. Devos, "Clinical experience with tight glucose control by intensive insulin therapy," *Crit. Care Med.*, vol. 35, no. 9, pp. S503–S507, Sep. 2007.
- [13] B. P. Kavanagh and K. C. McCowen, "Glycemic control in the ICU," New England J. Med., vol. 363, no. 26, pp. 2540–2546, Dec. 2010.
- [14] E. A. Vogler, "Protein adsorption in three dimensions," *Biomaterials*, vol. 33, no. 5, pp. 1201–1237, Feb. 2012.
- [15] L. Li, S. Chen, and S. Jiang, "Protein interactions with oligo(ethylene glycol) (OEG) self-assembled monolayers: OEG stability, surface packing density and protein adsorption," *J. Biomaterials Sci., Polym. Ed.*, vol. 18, no. 11, pp. 1415–1427, Jan. 2007.
- [16] E. Ostuni, R. G. Chapman, R. E. Holmlin, S. Takayama, and G. M. Whitesides, "A survey of structure-property relationships of surfaces that resist the adsorption of protein," *Langmuir*, vol. 17, no. 18, pp. 5605–5620, Sep. 2001.
- [17] Q. Yang et al., "Development of glucose sensor using gold nanoparticles and glucose-oxidase functionalized tapered fiber structure," *Plasmonics*, vol. 15, no. 3, pp. 841–848, Jun. 2020.
- [18] A. Kumari, V. Vyas, and S. Kumar, "Synthesis, characterization, and applications of gold nanoparticles in development of plasmonic optical fiber-based sensors," *Nanotechnology*, vol. 34, no. 4, Jan. 2023, Art. no. 042001.
- [19] S. K. Srivastava, V. Arora, S. Sapra, and B. D. Gupta, "Localized surface plasmon resonance-based fiber optic U-shaped biosensor for the detection of blood glucose," *Plasmonics*, vol. 7, no. 2, pp. 261–268, Jun. 2012.
- [20] S. A. Maier et al., Plasmonics: Fundamentals and Applications, vol. 1. New York, NY, USA: Springer, 2007.
- [21] C. F. Bohren and D. R. Huffman, Absorption and Scattering of Light by Small Particles. Hoboken, NJ, USA: Wiley, 2008.
- [22] K. M. Mayer and J. H. Hafner, "Localized surface plasmon resonance sensors," Chem. Rev., vol. 111, no. 6, pp. 3828–3857, Jun. 2011.
- [23] J. Dong, P. L. Carpinone, G. Pyrgiotakis, P. Demokritou, and B. M. Moudgil, "Synthesis of precision gold nanoparticles using Turkevich method," KONA Powder Part. J., vol. 37, pp. 224–232, 2020.

- [24] C. Ziegler and A. Eychmüller, "Seeded growth synthesis of uniform gold nanoparticles with diameters of 15–300 nm," J. Phys. Chem. C, vol. 115, no. 11, pp. 4502–4506, Mar. 2011.
- [25] H.-M. Kim, D. Hong Jeong, H.-Y. Lee, J.-H. Park, and S.-K. Lee, "Improved stability of gold nanoparticles on the optical fiber and their application to refractive index sensor based on localized surface plasmon resonance," Opt. Laser Technol., vol. 114, pp. 171–178, Jun. 2019.
- [26] P. Mondal, C. Guo, and J. L. Yarger, "Water soluble gold-polyaniline nanocomposite: A substrate for surface enhanced Raman scattering and catalyst for dye degradation," *Arabian J. Chem.*, vol. 13, no. 2, pp. 4009–4018, Feb. 2020.
- [27] T. K. Koo and M. Y. Li, "A guideline of selecting and reporting intraclass correlation coefficients for reliability research," *J. Chiropractic Med.*, vol. 15, no. 2, pp. 155–163, Jun. 2016.
- [28] S. Talukder, S. Kundu, and R. Kumar, "Dynamic calibration of nonlinear sensors with time-drifts and delays by Bayesian inference," 2022, arXiv:2208.13819.
- [29] Y. Li et al., "Immobilized optical fiber microprobe for selective and high sensitive glucose detection," *Sens. Actuators B, Chem.*, vol. 255, pp. 3004–3010, Feb. 2018.
- [30] B. Jiang et al., "Label-free glucose biosensor based on enzymatic graphene oxide-functionalized tilted fiber grating," Sens. Actuators B, Chem., vol. 254, pp. 1033–1039, Jan. 2018.
- [31] R. F. B. Turner, D. J. Harrison, R. V. Rajotte, and H. P. Baltes, "A biocompatible enzyme electrode for continuous in vivo glucose monitoring in whole blood," *Sens. Actuators B, Chem.*, vol. 1, nos. 1–6, pp. 561–564, Jan. 1990.
- [32] Y. Yonemori, E. Takahashi, H. Ren, T. Hayashi, and H. Endo, "Biosensor system for continuous glucose monitoring in fish," *Anal. Chim. Acta*, vol. 633, no. 1, pp. 90–96, Feb. 2009.
- [33] W. Zheng et al., "Highly-sensitive and reflective glucose sensor based on optical fiber surface plasmon resonance," *Microchem. J.*, vol. 157, Sep. 2020, Art. no. 105010. [Online]. Available: https://www. sciencedirect.com/science/article/pii/S0026265X19337154
- [34] J. Zhang, X. Mai, X. Hong, Y. Chen, and X. Li, "Optical fiber SPR biosensor with a solid-phase enzymatic reaction device for glucose detection," Sens. Actuators B, Chem., vol. 366, Sep. 2022, Art. no. 131984.
- [35] S. Liakat, K. A. Bors, L. Xu, C. M. Woods, J. Doyle, and C. F. Gmachl, "Noninvasive in vivo glucose sensing on human subjects using midinfrared light," *Biomed. Opt. Exp.*, vol. 5, no. 7, pp. 2397–2404, 2014.
- [36] C. Vrančić, N. Kröger, N. Gretz, S. Neudecker, A. Pucci, and W. Petrich, "A quantitative look inside the body: Minimally invasive infrared analysis in vivo," *Anal. Chem.*, vol. 86, no. 21, pp. 10511–10514, Nov. 2014.
- [37] M. Vettoretti, A. Facchinetti, S. Del Favero, G. Sparacino, and C. Cobelli, "Online calibration of glucose sensors from the measured current by a time-varying calibration function and Bayesian priors," *IEEE Trans. Biomed. Eng.*, vol. 63, no. 8, pp. 1631–1641, Aug. 2016.
- [38] S. Guerra, A. Facchinetti, G. Sparacino, G. D. Nicolao, and C. Cobelli, "Enhancing the accuracy of subcutaneous glucose sensors: A real-time deconvolution-based approach," *IEEE Trans. Biomed. Eng.*, vol. 59, no. 6, pp. 1658–1669, Jun. 2012.